

Alma Mater Studiorum Università di Bologna
Archivio istituzionale della ricerca

Dynamic behavior of a spring-powered micronozzle needle-free injector

This is the final peer-reviewed author's accepted manuscript (postprint) of the following publication:

Published Version:

Schoubben A., Cavicchi A., Barberini L., Faraon A., Berti M., Ricci M., et al. (2015). Dynamic behavior of a spring-powered micronozzle needle-free injector. INTERNATIONAL JOURNAL OF PHARMACEUTICS, 491(1-2), 91-98 [10.1016/j.ijpharm.2015.05.067].

Availability:

This version is available at: <https://hdl.handle.net/11585/703579> since: 2020-02-25

Published:

DOI: <http://doi.org/10.1016/j.ijpharm.2015.05.067>

Terms of use:

Some rights reserved. The terms and conditions for the reuse of this version of the manuscript are specified in the publishing policy. For all terms of use and more information see the publisher's website.

This item was downloaded from IRIS Università di Bologna (<https://cris.unibo.it/>).
When citing, please refer to the published version.

(Article begins on next page)

This is the final peer-reviewed accepted manuscript of: Aurélie Schoubben, Andrea Cavicchi, Lanfranco Barberini, Alessio Faraon, Marco Berti, Maurizio Ricci, Paolo Blasi, Lucio Postrioti. Dynamic behavior of a spring-powered micronozzle needle-free injector. Int. J. Pharm. 491 (2015) 91-98.

The final published version is available online at:
<https://www.sciencedirect.com/science/article/abs/pii/S0378517315004962#:~:text=https%3A//doi.org/10.1016/j.ijpharm.2015.05.067>

Rights / License:

The terms and conditions for the reuse of this version of the manuscript are specified in the publishing policy. For all terms of use and more information see the publisher's website.

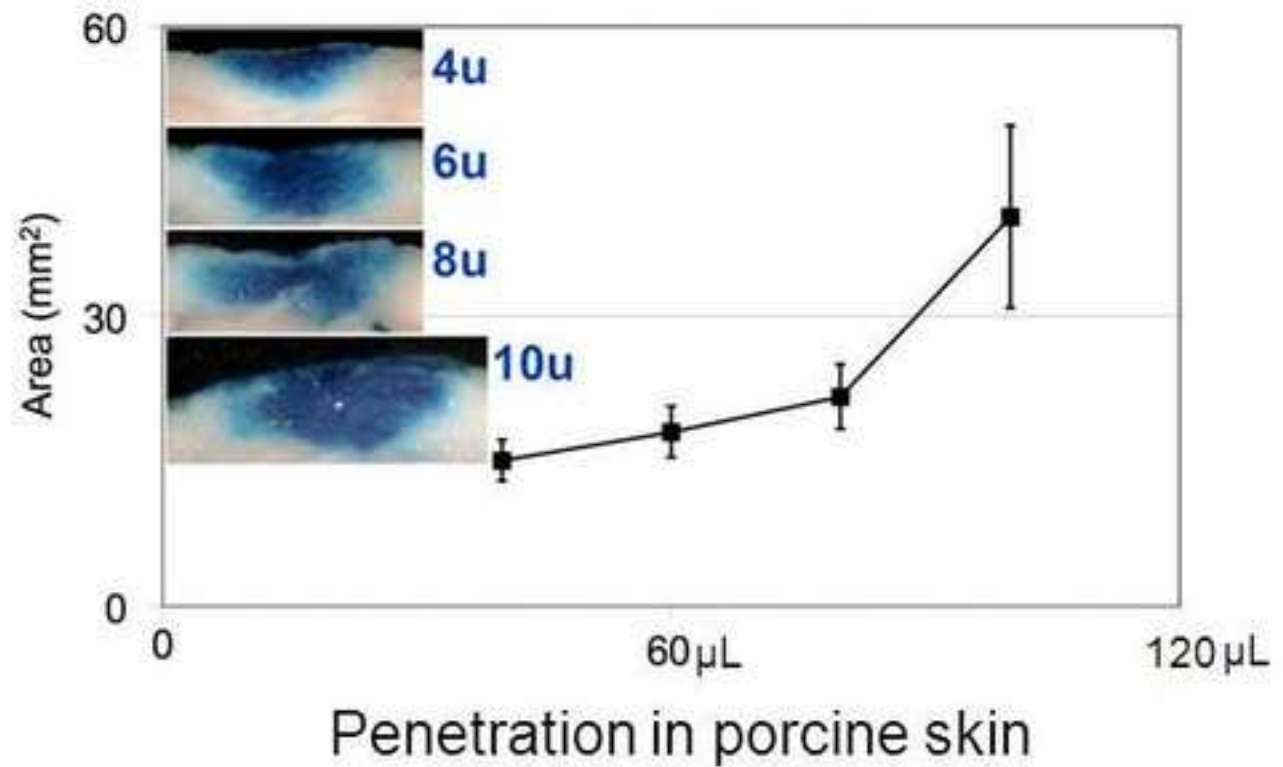
This item was downloaded from IRIS Università di Bologna (<https://cris.unibo.it/>)

When citing, please refer to the published version.

Spring-powered Micronozzle Needle-free Injector



Needle-free injector



1 **DYNAMIC BEHAVIOR OF A SPRING-POWERED MICRONOZZLE NEEDLE-FREE**
2 **INJECTOR**

3
4
5 Aurélie Schoubben¹, Andrea Cavicchi², Lanfranco Barberini³, Alessio Faraon⁴, Marco Berti⁴,
6 Maurizio Ricci¹, Paolo Blasi^{5*}, Lucio Postrioti^{2*}

7
8 ¹ Dipartimento di Scienze Farmaceutiche, Università degli Studi di Perugia, Perugia, Italy

9 ² Dipartimento di Ingegneria, Università degli Studi di Perugia, Perugia, Italy

10 ³ Dipartimento di Chimica, Biologia e Biotecnologie, Università degli Studi di Perugia, Perugia,
11 Italy

12 ⁴ Brovedani Group, San Vito al Tagliamento, Italy

13 ⁵ School of Pharmacy, University of Camerino, Via Sant’Agostino 1, 62032, Camerino, Italy.

14
15
16
17
18
19
20 * Corresponding Authors:

21 Paolo BLASI, e-mail: paolo.blasi@unicam.it; phone +39 0737402289, fax: +39 0737637345.

22 Lucio POSTRIOTI, e-mail: lucio.postrioti@unipg.it; Phone/fax: +39 0755853733

30 **Abstract**

31 Conventional injection is still the leading method to deliver macromolecular therapeutics. Needle
32 injection is considered a low compliance administration strategy, principally due to pain and needle
33 phobia. This has fostered the research on the development of alternative strategies to circumvent the
34 skin barrier. Among needle-free drug delivery methods, jet injection is an old strategy with great
35 potential not yet completely disclosed. Here, the design, engineering and dynamic behavior of a
36 novel spring-powered micronozzle needle-free injector is presented. Fluid mechanics was first
37 studied in air to calculate jet force and speed as well as injection duration in different conditions.
38 Polyacrylamide gel was used to simulate a soft tissue and to investigate the jet evolution over time
39 of different injected doses. Finally, *ex vivo* characterization was carried out on pig skin. Results
40 evidenced a direct dependence of the force, velocity, and duration with the injection volume. The
41 model material allowed individuating the different steps of jet penetration and to attempt a
42 mechanistic explanation. A different behavior has been recorded in the skin with interesting
43 findings for subcutaneous and/or dermal delivery. Peculiar features with respect to existing jet
44 injectors confers to this device good potentiality for a future clinical application.

45

46

47

48

49

50

51

52

53 **Keywords:** spring-powered needle-free injectors, jet injectors, micronozzle, transdermal delivery,
54 and insulin.

55

56	List of symbols and abbreviations
57	API, active pharmaceutical ingredient;
58	v , speed at the nozzle exit section;
59	m , injected mass;
60	Δt , injection duration;
61	ρ , density of the solution
62	A , nozzle outflow section;
63	F , force;
64	p , pressure;
65	Δy , distance between the nozzle and the target;
66	$\Delta t_{(n \rightarrow t)}$, time of flight from nozzle to target;
67	L_t , penetration depth in pig skin (mm);
68	L_m , distance from the skin surface and the maximum width;
69	Q , volumetric flow rate;
70	μ , dynamic viscosity;
71	L , needle length;
72	D , needle bore diameter;
73	A_s , syringe stopper area;
74	C_d , discharge coefficient.
75	

76 1. Introduction

77 Conventional injection, syringe provided with needle, is at the moment the leading method to
78 deliver macromolecular therapeutics. Transdermal drug delivery offers a number of advantages,
79 especially when biological macromolecules are the therapeutics to be delivered (Prausnitz and
80 Langer 2008). Needle injection is considered a low compliance administration strategy, particularly
81 when applied to chronic therapies. Pain during administration and needle phobia are the factors
82 limiting its compliance. This has fostered the research on the development of new strategies for
83 transdermal delivery: these include formulation strategies and devices able to circumvent the skin
84 barrier avoiding conventional needles.

85 Formulation strategies comprise the addition of penetration enhancer (i.e., additives able to reduce
86 the skin barrier proprieties) (Williams and Barry 2004) or the inclusion of the active pharmaceutical
87 ingredient (API) in a carrier able to cross the skin (Cevc 2004). Pro-drug approach has been also
88 found useful but API chemical modification is not always feasible (Puglia et al. 2006).

89 Devices capable to puncture the skin and deliver therapeutics without the use of a conventional
90 needle (e.g., needle-free injectors, micro needles) are a reliable alternative to conventional
91 injections (Arora et al. 2007; van der Maaden et al. 2012; Xiang et al. 2013). Needle-free jet
92 injectors have been conceived to minimize pain and inconvenience in parenteral therapy. Invented
93 more than a century ago, liquid jet injectors were firstly used in clinics for mass immunization only
94 in the 1950's (Mitragotri 2012).

95 The basic components of a liquid jet injector are a compressed gas or a spring, a piston, a
96 compartment where the formulation is loaded, and a nozzle. These devices use the gas or the spring
97 as power source to push the piston that impress a pressure to the liquid formulation that, as a
98 reaction, is ejected through the nozzle orifice at high velocity ($v > 100$ m/s). Nozzle orifices have
99 been produced with diameters ranging from 76 to 360 μm but the most used devices had orifice
100 diameter of about 150 μm (Mitragotri 2013). The liquid jet pierces the *stratum corneum* delivering
101 the established formulation volume subcutaneously. From the engineering point of view, they are
102 easy to produce and relatively cheap because neither electrical power nor electronic parts are
103 required. From the clinical side, they are easy to handle, are applicable virtually to all liquid
104 formulations and may improve their pharmacokinetics (Schramm and Mitragotri 2002).

105 Paradoxically, one of the drawbacks that seems to limit the large clinical use of needle-free jet
106 injectors seems to be the pain but this issue is still controversial (Schneider et al. 1994; Zsigmond

107 2002). More critical are the inconsistency of formulation penetration and the pool out of liquid on
108 the skin (Mitragotri 2012). The latter limits intra- and inter-individual reproducibility of the key
109 pharmacokinetics parameters with obvious issues on formulation bioequivalence. This
110 inconsistency seems to be device related because some of them have shown even better
111 pharmacokinetic and pharmacodynamic parameters than conventional injection (Engwerda et al.
112 2011; Engwerda et al. 2013).

113 Most of the mentioned drawbacks are due to the limited number of systematic studies on the key
114 parameters involved in jet formation, skin penetration and drug delivery to tissue as well as the lack
115 of studies aimed at crossing these parameters with clinical data.

116 One possible solution to the pain generated by the jet could be the use of smaller orifice (i.e., 80
117 μm) to generate a high-velocity microjet ($v > 100 \text{ m/s}$). This solution has been proposed and
118 validated for the delivery of nanoliter volumes (Arora et al. 2007). Here we propose a novel device
119 provided with a micronozzle for medium volume skin delivery that could cover the gap between
120 microjets and conventional jet injectors.

121 The design (Figure 1) and the full characterization of the dynamic behavior of a novel spring-
122 powered needle-free liquid jet injector are reported below.

123

124 2. Materials and methods

125 2.1. Materials

126 Acrylamide, bis-acrylamide, tetramethylethylenediamine and ammonium persulfate were purchased
127 from Bio-Rad Laboratories (Segrate, Italy) while methylene blue was obtained by Sigma (Milan,
128 Italy).

129 Porcine skin was kindly provided by the Centro Macellazione Carne (Ponte San Giovanni, Italy).

130 The needle-free injector mounted with an 80 µm nozzle was produced and provided by Brovedani
131 spa (San Vito al Tagliamento, Italy). All other reagents and products were of the highest grade
132 commercially available and used as received.

133 2.2. Dynamic performance characterization

134 The injector was characterized in terms of dynamic performances by loading and injecting different
135 volumes of distilled water (40, 80 and 120 µL). Each test was repeated 5 times and the following
136 data were recorded:

- 137 - Mass of liquid shot by the injector, computed as a difference of device weight, before and after
138 the shot;
- 139 - Impact force on a target positioned at 17 mm from the nozzle hole. The impact force was
140 measured with a high-sensitivity, piezoelectric force sensor (Kistler Type 9215, Kistler
141 Holding AG, Winterthur, Switzerland). From these data it was possible to gain information
142 about the momentum flux through the nozzle hole and the duration of the injection process.

143 2.2.1. Average speed measurement

144 The average outlet speed from the nozzle was computed knowing time duration of the shot and the
145 mass of the volume injected as reported in the following equation;

146

$$147 \frac{m}{\Delta t} = \rho A v \rightarrow v = \frac{m}{\rho A \Delta t}$$

Equation 1

148

149 where v is the speed at the nozzle exit section, m is the injected mass, Δt the injection duration, ρ
150 the density of the solution and A the nozzle outflow section (Arora et al. 2007; Schramm and
151 Mitragotri 2002; Schramm-Baxter and Mitragotri 2004a).

152

153 **2.2.2. Impact force and instantaneous velocity measures**

154 The nozzle outflow velocity was calculated from the force signal. The impact force on the target is
155 equal to the momentum flux through the nozzle hole, if the following hypotheses are verified
156 (Postrioti and Battistoni 2010; Postrioti et al. 2012):

- 157 - Steady flow;
- 158 - The jet is orthogonally deviated by the target, so to lose at the impact its velocity component
159 directed towards the target itself.

160 The maximum, minimum, and mean force values as well as the corresponding speed values have
161 been calculated using the following equation;

$$162 \quad F = \rho A v^2 \rightarrow v = \sqrt{\frac{F}{\rho A}} \quad \text{Equation 2}$$

163

164 The pressure into the nozzle can be evaluated applying Bernoulli equation upstream and
165 downstream the nozzle hole. The maximum pressure was calculated from the force signal using the
166 momentum equation.

167

$$168 \quad \frac{p}{\rho} + \frac{v^2}{2} = \text{cost.} \rightarrow p = \frac{\rho v^2}{2} = \frac{F}{2A} \quad \text{Equation 3}$$

169

170

171

172

173 2.2.3. *Jet tip speed*

174 The jet tip speed was estimated from the video analysis. For every acquisition two frames were
175 extracted: the first at the beginning of the injection and the second at the impact against the target.
176 Knowing the sequence number of the frames and the time delay between two consecutive frames
177 (equal to 1/fps), the time spent by the jet tip to reach the target was defined. The distance covered in
178 mm was the measure in pixel multiplied by the image scale factor. So the average jet speed is:

179

$$180 \quad v = \frac{\Delta y}{\Delta t(n \rightarrow t)} \quad \text{Equation 4}$$

181

182 2.3. *In vitro motion studies*

183 2.3.1. *Polyacrylamide gel preparation*

184 Polyacrylamide gel was used as a model soft material to mimic human epidermal tissue texture
185 (Schramm-Baxter et al. 2004; Stachowiak et al. 2009). Acrylamide and bis-acrylamide were
186 solubilized in distilled water at 4 and 0.16% (w/v), respectively. Initiators (N,N,N',N'-
187 tetramethylethylenediamine, 0.005% w/v; ammonium persulfate, 0.075% w/v) were added to the
188 solution that was vigorously shaken and immediately poured in round bottom glass tubes (diameter,
189 12 mm; length, 55 mm; volume, 4.5 mL) and left polymerize under daylight. Complete
190 polymerization was achieved after 1 hour.

191

192 2.3.2. *Experimental setup*

193 The analysis of the spray evolving in gel was based on a imaging system in backlight arrangement.
194 The glass test tube containing the gel was positioned between the illumination system and the high
195 speed camera. The set-up elements were mounted on a linear guide so to adjust their relative
196 positions. The injector was loaded with methylene blue solution (1% w/v) to obtain a proper
197 contrast between liquid and gel in the acquired images and the jet evolution in gel was recorded
198 using a high speed camera (Phantom[®] v711, Vision Research, Wayn, NJ, USA). The high speed

199 camera was equipped with a Nikkor 200 mm objective (Nikon), operating at high frequency (1600
200 frame/s) set at 60 μ s exposure time. The lighting system needed for this exposure time consisted of a
201 LED matrix (48 x SMD 505, 12V) and a light diffuser. The glass tube containing the gel was placed
202 between the LED panel and the camera. Different volumes of methylene blue solution (40, 60, 80,
203 100 and 120 μ L), corresponding to different insulin units (4, 6, 8, 10 and 12 units), were injected
204 and each injection was repeated 5 times.

205

206 **2.3.3. Image acquisition and post-processing**

207 Every acquisition generated a video composed of about 1000 frames acquired at a constant frame
208 rate and covering an entire injection process. The off-line analysis of the acquired video allowed the
209 detection of the injection process beginning that is assumed as time-zero for the following analyses.
210 After the time-zero frame detection, selected frames were extracted from the video to quantitatively
211 analyze the process evolution. The extracted frames time step was short at the beginning of the
212 process, when the jet evolved quickly. Once steady flow was reached, the time step became longer.
213 The single frame analysis was stopped at the injection process end. The first frame in which the
214 liquid column detached from the nozzle assumed the timing of the injection end.

215 Each of the extracted frames was converted in a “jpg” format image and used for the quantitative
216 analysis, by which the spray tip penetration time-history along with the jet width and area were
217 computed by means of self-developed image analysis software written in LabVIEW Vision
218 environment. In particular, each image was converted in a binary file setting a grey threshold level
219 above which or under which the pixel was white for the gel or black for methylene blue. This
220 procedure was required to convert a real-world image in grey levels to a black and white pixel
221 image, on which it has been possible to perform geometrical measurements after color inversion to
222 obtain a white-on-black image.

223

224 **2.3.4. Measurements**

225 The first geometrical measurement was focused on the computation of the white pixels, as an
226 approximation of the jet volume, with the assumption of an axial-symmetric jet evolution. The jet
227 penetration was determined defining the nozzle hole coordinates as it appeared in the sequence and
228 moving a measuring bar starting from the opposite boundary of the image looking for the position

229 in which the measuring bar was tangent to the jet boundary. In a conceptually similar manner, the
230 software computed the jet width as the sum of its length in the left and right directions. The time
231 evolution of these quantities gave important knowledge about the spray behavior in terms of
232 tendency to correctly penetrate the gel bulk and to form a well-defined sac of the injected liquid in
233 the gel mass.

234

235 ***2.4. Ex vivo characterization***

236 Porcine skin was employed to study the depth of the penetration reached by the solution injected
237 and the relative area developed (longitudinal section). Methylene blue solution (1% w/v) was used
238 since it consents to easily distinguish the portion of the tissue reached by the solution injected from
239 the rest of the tissue. Just after injection, the skin sample was frozen using a cryospray
240 (Histofreezer[®], OraSure Technologies, Inc., Bethlehem, PA, USA) and successively cut
241 longitudinally at the injection point. The sections were photographed using stereoscope (Leica
242 WILD M32 with WILD PLANIX ocular) equipped with a camera (Leica DFC 320). From the
243 photomicrographs, three different determinations were made: the measurement of the penetration
244 depth (L_t), the distance from the skin surface corresponding to maximum width (L_m) and the
245 estimation of the injected area (Figure 2). Different volumes of methylene blue solution
246 (corresponding to 4, 6, 8 and 10 insulin units) were injected and the results were expressed as the
247 mean of 10 measurements \pm standard deviation.

248

249 3. Results and discussion

250 3.1. Needle-free injector dynamic performances

251 To determine the average fluid outcome velocity (Eq. 1), the injection duration was deduced from
252 the spray impact force signal profiles (Figure 3). The actual injection duration was easily calculable
253 since the signal start and end were well definite. The maximum and minimum forces and the
254 duration of the injection were extracted from Figure 3 as the signal value at start and end points
255 (Table 1). In the evaluation of the fluid outcome velocity, the initial force peak was ignored. The
256 first force peak is actually due to the impact phenomenon onset, during which the steady flow
257 condition cannot be considered true. Only in steady flow conditions, the impact force can be
258 assumed as corresponding to the spray momentum flux.

259 The device performed a regular injection that produced a force signal with very short start and end
260 ramps and a definite steady value in the middle. The spring pre-charge force was proportional to
261 fluid volume to be injected. This behavior is due to the device engineering. The reservoir has a
262 variable volume that can load from 20 to 160 μL of formulation. A revolving system in the back of
263 the device is used to load the formulation (Figure 1). At each revolution the piston steps back
264 increasing the volume of the loading chamber of 20 μL and the spring is compressed
265 correspondingly. As a consequence, the tested needle-free device is characterized by an increase of
266 the spring compression with the loading (injection volume). This implies a rise of the spray velocity
267 and momentum flux with the injected volume. This trend was clearly confirmed by the
268 experimental spray impact force profiles, which evidenced not only an increase of the injection
269 process duration with the injected volume (Figure 3) but also of the impact force intensity (Table 1).

270 The speed values calculated using equations 1 and 2 gave similar values with a difference lower
271 than 10%, underlining the robustness of the methods employed (Table 2).

272 As expected, the speed evaluated using the video analysis was lower (Table 2) since the jet tip
273 penetration is a phenomenon mostly controlled by drag effects exerted by the gel on the injected
274 liquid column. All values showed an increase of the speed with the increase of the volume injected.
275 In comparison with other devices reported in literature (Stachowiak et al. 2009), the device
276 presented here produced a faster jet.

277 The pressure into the nozzle increased with the increase of the volume loaded (Table 2). This is the
278 consequence of the spring pre-charge force increase that is directly proportional to the volume
279 loaded into the system. Maximum pressure values are generally higher than the reported for other

280 needle-free injectors (Schramm and Mitragotri 2002). Obviously, differences can be found in the
281 different power source and nozzle diameter; both responsible for the generation of different
282 pressures.

283 Interestingly, device performances should not change significantly by increasing formulation
284 viscosity (Fry 2014). Highly viscous liquid pharmaceutical formulations are generally difficult to
285 handle with conventional syringes because of syringeability and injectability issues (Cilurzo et al.
286 2011). The large availability of high molecular weight therapeutic proteins produced with the
287 recombinant DNA technology has renewed the interest for needle-free injectors. Large
288 macromolecules at the desired dose may produce highly viscous solutions difficult to deliver with
289 conventional strategies. In the viscosity range of interest, needle-free injector performances are
290 mainly unaffected (Cilurzo et al. 2011).

291 In a conventional syringe provided with needle, the force necessary to extrude the formulation is
292 proportional to its viscosity as shown in the Hagen-Poiseuille equation;

293

$$294 \quad F = \frac{128 Q \mu L A_s}{\pi D^4} \quad \text{Equation 5}$$

295

296 where F is the syringe stopper force, Q the volumetric flow rate, μ the dynamic viscosity, L the
297 needle length, D the needle bore diameter and A_s the syringe stopper area.

298 The force needed to extrude a liquid formulation from a needle-free device may be calculated
299 rearranging the Bernoulli equation as follow;

300

$$301 \quad F = 2 \rho A_s \left(\frac{4 Q}{C_d \pi D^2} \right)^2 \quad \text{Equation 6}$$

302

303 where ρ is the fluid density and C_d the discharge coefficient.

304 The sole explicit fluid property in the equation (Eq. 6) is ρ that generally is very close to 1. To be
305 honest, fluid viscosity is hidden in C_d but, in the range of viscosities of pharmaceutical interest, its
306 contribution may be considered negligible.

307

308 **3.2. *In vitro* motion data**

309 To perform a high-speed video analysis, the key condition is that the medium used needs to be
310 completely transparent to detect the injected fluid with an acceptable contrast. Therefore, the great
311 advantage of using gel is its transparency to the visible light.

312 Sample sequences show that the jet initially goes straight into the gel in less than 1 ms and then
313 accumulates forming a sphere or sac in the gel bulk that grows progressively (Figure 4).

314 The depth of linear penetration did not change much with the increase of the volume injected
315 indicating an initial loss of momentum flux by the jet (first 10 mm). Figure 5 shows the profiles of
316 areas evolved, that are intended just as an approximation of the injected volumes since the images
317 analyzed were two-dimensional. This approximation is conceivable due to the anisotropic character
318 of a randomly cross-linked gel.

319 The measured jet area rises linearly up to its maximum value that was reached after an increasing
320 time-lapse with the increasing dose injected. With 4 units, the maximum area ($\sim 30 \text{ mm}^2$) was
321 reached after about 30 ms, while it was attained after about 120 ms ($\sim 80 \text{ mm}^2$) for the highest dose
322 (Figure 5a). From the results, it is also possible to conclude that the duration of the injection event
323 increases linearly with the increase of the volume injected. The jet penetration computation is
324 probably one of the most important features to characterize the spray evolution. The penetration
325 curves rose very fast during the first milliseconds of the injection; then the increase became very
326 slow. The injector gave similar results in terms of penetration (8-10 mm) for all the volumes
327 injected (only data for 80 μL are shown) but the highest dose (120 μL) where a small increase of
328 the penetration depth was observed ($\sim 14 \text{ mm}$) (Figure 5b).

329 In the first laps of the injection (until 20-30 ms), the injector had a wide development in the
330 analyzed direction, possibly due to its relatively limited penetration (Figure 6). The jet development
331 was regular and methylene blue accumulates in a sort of regular sphere that grew up progressively.
332 This regular behavior seems to be due to the small nozzle diameter (80 μm) combined with the high
333 actuation pressure which together cause the jet to act as a thin needle, easily penetrating in the first

334 stratum of the gel, preserving here its shape but quickly losing its momentum later on. As shown in
335 Figure 6, the right side and the left side of the sphere evolved in the same mode.

336 A mechanistic explanation of jet penetration in polyacrylamide gel has been attempted [13]. During
337 the first 2 ms after actuation, 3 different phases have been individuated: erosion (~ 0.2 ms) followed
338 by about 0.8 ms of stagnation and diffusion that last until the complete delivery (Schramm-Baxter et
339 al. 2004). Differently from previous reported data (Schramm-Baxter and Mitragotri 2004;
340 Schramm-Baxter et al. 2004; Stachowiak et al 2009), the third phase, called diffusion, generated a
341 sphere with an additional structure growing up at later time points, leading to a jellyfish-like
342 geometrical form (Figure 4). This behavior could be due to a combination of the gel elastic
343 properties and the size of the tube. During diffusion the sphere grows reaching a size of the same
344 order of magnitude of the glass tube diameter. Being a forced diffusion, it can be speculated that the
345 equatorial elasticity of the gel decrease while approaching the glass, generating a turbulent back-
346 flow escaping the sphere in its upper part. Differences in poly (acrylamide) gel elasticity have been
347 recorded individuating a position-dependent (distance from the bottom) elastic modulus (Durmaz
348 and Okay 2011). Polyacrylamide films seem to have elasticity correlated with the film thickness:
349 thinner is the film lower is the elastic modulus (Buxboim et al. 2010).

350

351 **3.3. *Ex vivo* characterization**

352 Figure 7a shows that the area of the solution injected in porcine skin linearly increases from 15 to
353 22 mm^2 injecting the equivalent of 40, 60, and $80 \text{ }\mu\text{L}$ of methylene blue (1% w/v) aqueous solution.
354 Similarly to what observed with the measurement of the penetration depth (Figure 7b), the injection
355 of $100 \text{ }\mu\text{L}$ produced the highest area (40 mm^2) breaking the linear increase observed with the first 3
356 doses injected. The reproducibility was high if considering the possible variability that can be
357 obtained working with biological tissues. This behavior correlates with what was observed during
358 the force determination study.

359 Figure 7b shows that the penetration depth linearly increases from 2.7 to 3.2 mm by injecting 40,
360 60, and $80 \text{ }\mu\text{L}$ of methylene blue (1% w/v) aqueous solution. The injection of $100 \text{ }\mu\text{L}$ produced the
361 deepest penetration (4.4 mm) without following the linearity observed with lower dosages. This
362 behavior is probably due to the mechanical system triggering the injection that has progressively
363 higher strength increasing the dose charged. High reproducibility was observed for the first 3 doses
364 injected.

365 L_m shows a linear increase from about 0.5 to 1.5 mm when delivering 40 to 100 μ L with a nozzle of
366 80 μ m in diameter (Figure 7c). Higher values of L_m were obtained using a device mounting 152 μ m
367 nozzle and extruding at the same velocity of the injectors under investigation (Schramm-Baxter et
368 al. 2004). Low L_t and L_m values are interesting when a subcutaneous or a dermal deposition is the
369 aim of the administration.

370 Comparing the injections in polyacrylamide (Figure 4) and in pigskin (Figure 8, insert), it can be
371 hypothesized a different jet evolution. In pigskin, the colored solution did not form neither a sphere,
372 nor a jellyfish geometric form (Figure 7, insert). Epidermis and dermis have well-structured extra
373 cellular matrices with an abundance of longitudinal fibers (parallel to the skin surface). It seems that
374 the jet momentum was lost very fast and, because of fibers orientation, lateral diffusion is easily
375 achieved (Figure 7, insert).

376

377 **4. Conclusions**

378 A novel and simple micronozzle needle-free injector has been built and characterized. Due to the
379 small nozzle diameter it should not cause pain during injection. The device showed efficiency and
380 reproducibility in delivering liquid formulations subcutaneously or in the intradermal space. The jet
381 force and velocity directly increases with the volume loaded so generating an adequate penetration
382 and diffusion for all the injected volumes. This should guarantee a complete and rapid absorption
383 even for high volumes.

384

385

386

387

388

389 **Acknowledge**

390 Brovedani Group provided the needle-free injector and financed the research.

391

392 **References**

- 393 Arora, A., Hakim, I., Baxter, J., Rathnasingham, R., Srinivasan, R., Fletcher, D.A., Mitragotri, S.,
394 2007. Needle-free delivery of macromolecules across the skin by nanoliter-volume pulsed
395 microjets. *Proc. Natl. Acad. Sci. USA*. 104 (2007) 4255-4260.
- 396 Buxboim, A., Rajagopal, K., Brown, A.E.X., Discher, D.E., 2010. How deeply cells feel: methods
397 for thin gels. *J. Phys. Condens. Matter*. 22, 194116-194125.
- 398 Cevc, G., 2004. Lipid vesicles and other colloids as drug carriers on the skin. *Adv. Drug Deliv.*
399 *Rev.* 56, 675-711.
- 400 Cilurzo, F., Selmin, F., Minghetti, P., Adami, M., Bertoni, E., Lauria, S., Montanari, L., 2011.
401 Injectability evaluation: an open issue. *AAPS PharmSciTech* 12, Article No. 2.
- 402 Durmaz, S., Okay, O., 2011. Inhomogeneities in poly(acrylamide) gels: position-dependent elastic
403 modulus measurements. *Polym. Bull.* 46, 409-418.
- 404 Engwerda, E.E.C., Abbink, E.J., Tack, C.J., de Galan, B.E., 2011. Improved pharmacokinetic and
405 pharmacodynamic profile of rapid-acting insulin using needle-free jet injection technology.
406 *Diabetes Care* 34, 1804-1808.
- 407 Engwerda, E.E.C., Tack, C.J., de Galan, B.E., 2013. Needle-Free Jet Injection of Rapid-Acting
408 Insulin Improves Early Postprandial Glucose Control in Patients With Diabetes. *Diabetes Care* 36,
409 3436-3441.
- 410 Fry, A., Injecting highly viscous drugs. 2014. *Pharm. Tech. Europe* 26, 30-32.
- 411 Mitragotri, S., Devices for overcoming biological barriers: the use of physical force, 2013. *Adv.*
412 *Drug Deliv. Rev.* 65, 100-103.
- 413 Mitragotri, S., Mechanical disruption of skin barrier for vaccine delivery, 2012. *Drug Deliv. Sys.*
414 27, 202-212.
- 415 Postrioti, L., Battistoni, M., 2010. Evaluation of diesel spray momentum flux in transient flow
416 conditions. *SAE Technical Paper* 2010-01-2244.
- 417 Postrioti, L., Mariani, F., Battistoni, M., 2012. Experimental and numerical momentum flux
418 evaluation of high pressure diesel spray. *Fuel* 98, 149-163.

419 Prausnitz, M.R., Langer, R., 2008. Transdermal drug delivery. *Nat. Biotechnol.* 26, 1261-1268.

420 Puglia, C., Filosa, R., Peduto, A., de Caprariis, P., Rizza, L., Bonina, F., Blasi, P., 2006. Evaluation
421 of alternative strategies to optimize ketorolac transdermal delivery, *AAPS PharmSciTech* 7, Article
422 64.

423 Schneider, U., Birnbacher, R., Schober, E., 1994. Painfulness of needle and jet injection in children
424 with diabetes mellitus. *Eur. J. Pediatr.* 153, 409-410.

425 Schramm, J., Mitragotri, S., 2002. Transdermal drug delivery by jet injectors: energetics of jet
426 formation and penetration. *Pharm. Res.* 19, 1673-1679.

427 Schramm-Baxter, J., Katrencik, J., Mitragotri, S., 2004. Jet injection into polyacrylamide gels:
428 investigation of jet injection mechanics. *J. Biomech.* 37, 1181-1188.

429 Schramm-Baxter, J., Mitragotri, S., 2004. Needle-free jet injections: dependence of jet penetration
430 and dispersion in the skin on jet power. *J. Control. Release* 97, 527-535.

431 Stachowiak, J.C., Li, T.H., Arora, A., Mitragotri, S., Fletcher, D.A., 2009. Dynamic control of
432 needle-free jet injection. *J. Control. Release* 135, 104-112.

433 van der Maaden, K., Jiskoot, W., Bouwstra, J., 2012. Microneedle technologies for (trans)dermal
434 drug and vaccine delivery. *J. Control. Release* 161, 645-655.

435 Williams, A.C., Barry, B.W., 2004. Penetration enhancers. *Adv. Drug Deliv. Rev.* 56, 603-618.

436 Xiang, Z., Wang, H., Pant. A., Pastorin. G., Lee, C., 2013. Development of vertical SU-8
437 microneedles for transdermal drug delivery by double drawing lithography technology.
438 *Biomicrofluidics* 7, 066501.

439 Zsigmond, E.K., 2002. Jet anesthesia and jet local anesthesia for the 21st century. *J. Natl. Med.*
440 *Assoc.* 94, 1004-1006.

Table 1. Maximum and minimum force signals and injection duration obtained with different volumes.

Volume (μL)	Force (N)		Δt (s)
	Maximum	Minimum	
40	0.1318	0.1012	0.0456
80	0.1548	0.1076	0.0912
120	0.1792	0.1174	0.1344

Table 2. Speed and pressure data calculated using different equations.

Volume (μL)	Speed (m/s)					Maximum pressure (bar)
	Eq. 1	Eq. 2			Eq. 4	Eq. 3
		Maximum	Minimum	Mean		
40	184.8	182.1	159.5	170.8	53.97	165.7
80	190.8	197.3	164.5	180.9	59.22	194.7
120	196.2	212.3	171.8	192.1	61.93	225.3

Figure captions

Figure 1. Design of the Brovedani Nebulizer.

Figure 2. Photomicrograph of porcine skin longitudinal sections injected with methylene blue using the needle-free injector and representation of the method used to estimate methylene blue area. a) photomicrograph of porcine skin longitudinal sections injected with methylene blue using the needle-free injector and indication on how L_t and L_m were determined, b) photomicrograph transformed in black and white; c) quantification of the area of deposition (in red).

Figure 3. Impact force signal profiles obtained injecting 40, 80 and 120 μL of methylene blue (1% w/v) aqueous solution.

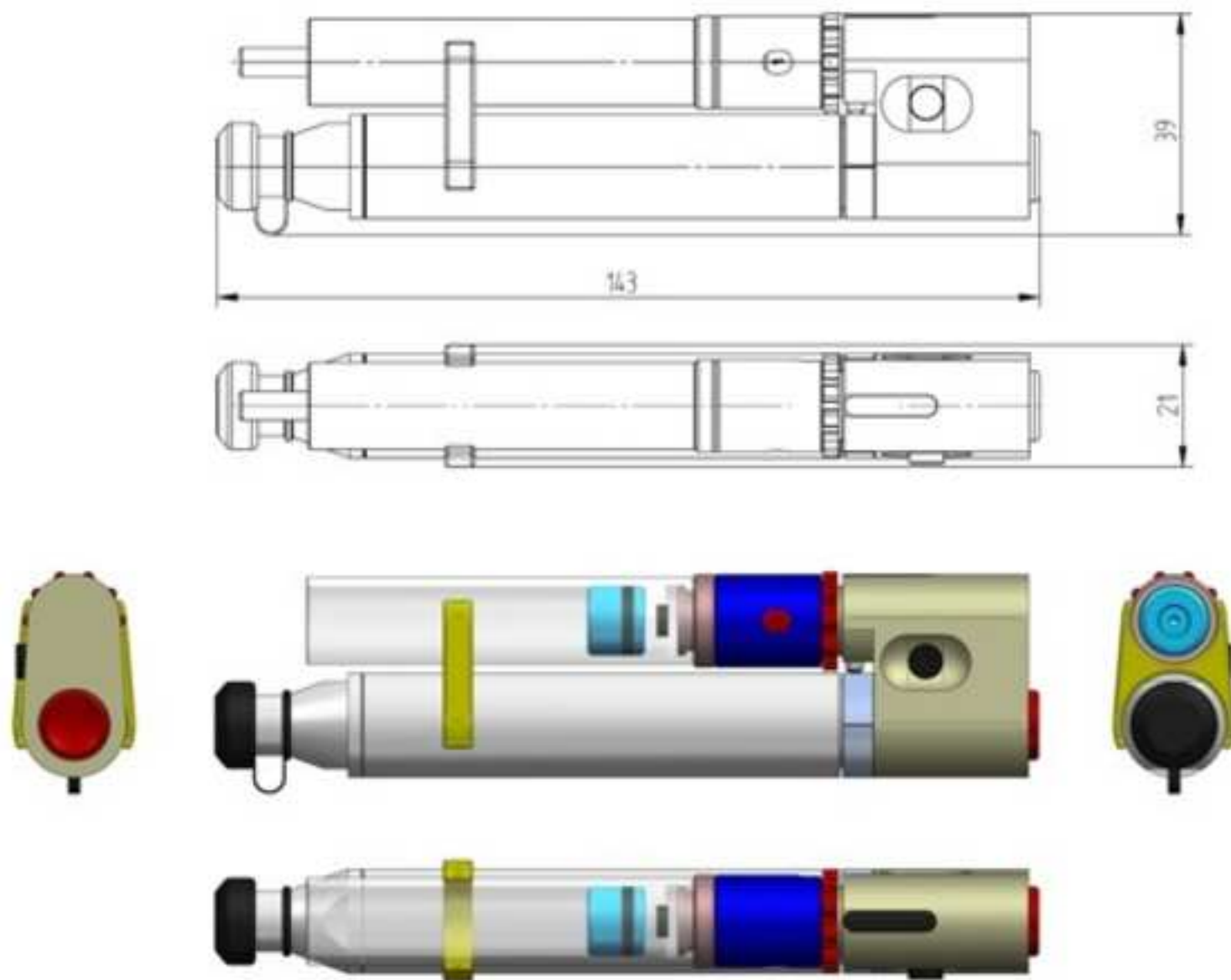
Figure 4. Frame sequence obtained with the needle-free injector by injecting 60 μL of methylene blue (1% w/v) aqueous solution.

Figure 5. (a) Area profiles obtained injecting 40, 60, 80, 100 and 120 μL of methylene blue (1% w/v) aqueous solution in polyacrylamide gel. **(b)** Depth of penetration profiles obtained injecting 80 and 120 μL of methylene blue (1% w/v) aqueous solution in polyacrylamide gel.

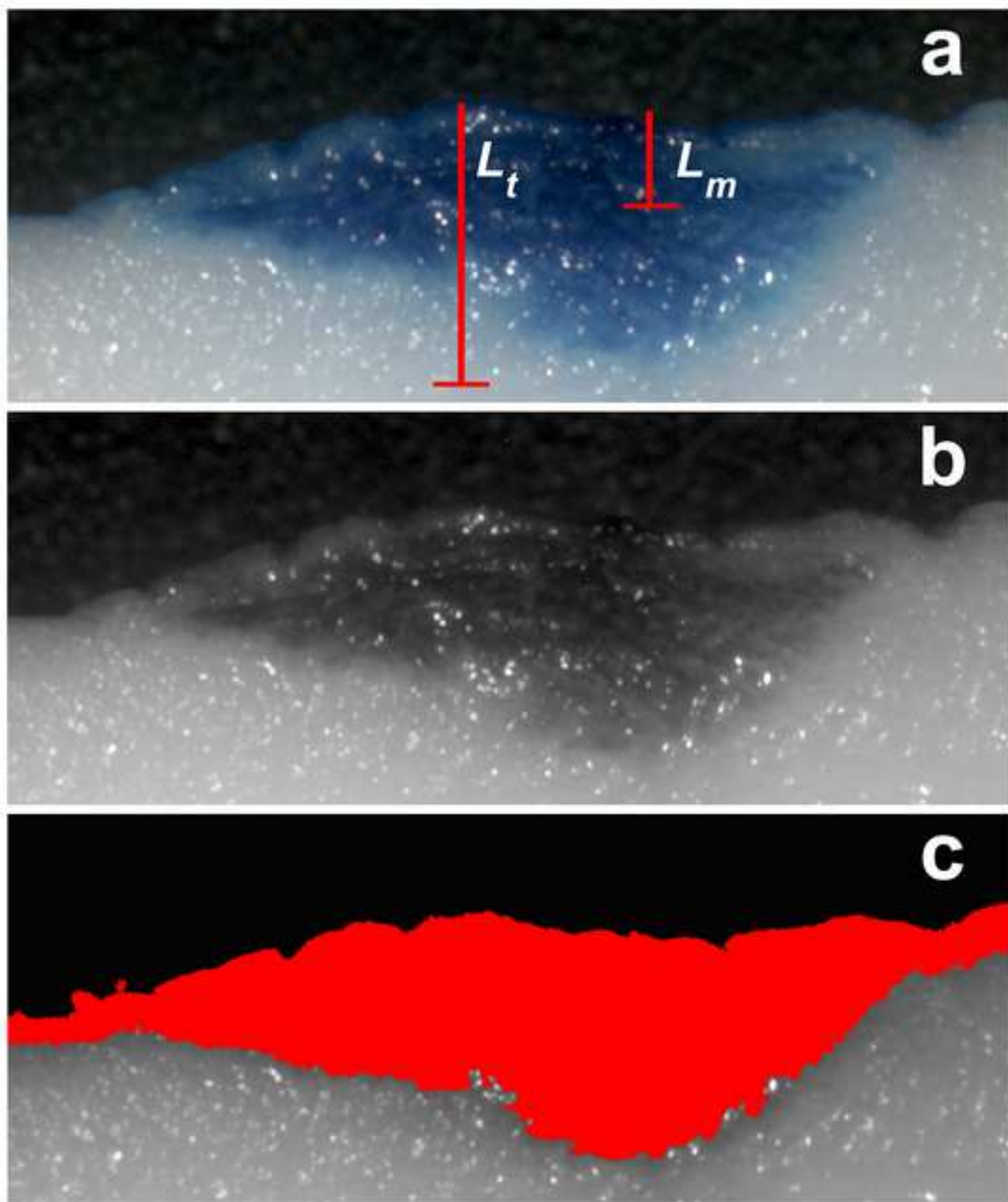
Figure 6. Left and right width profiles of the area obtained injecting 40, 60, 80, 100 and 120 μL of methylene blue (1% w/v) aqueous solution (from up to down) in polyacrylamide gel.

Figure 7. Plots of different measures done on porcine skin injected with 40, 60, 80, and 100 μL of methylene blue (1% w/v) aqueous solution. **Insert:** Photomicrographs of porcine skin longitudinal sections after injection 40, 60, 80, and 100 μL of methylene blue (1% w/v) aqueous solution, corresponding to 4, 6, 8 and 10 insulin units. **(a)** Area of penetration profiles; **(b)** maximum depths (L_t) reached by the injected solutions; **(c)** distance from the skin surface to the maximum width reached in the skin.

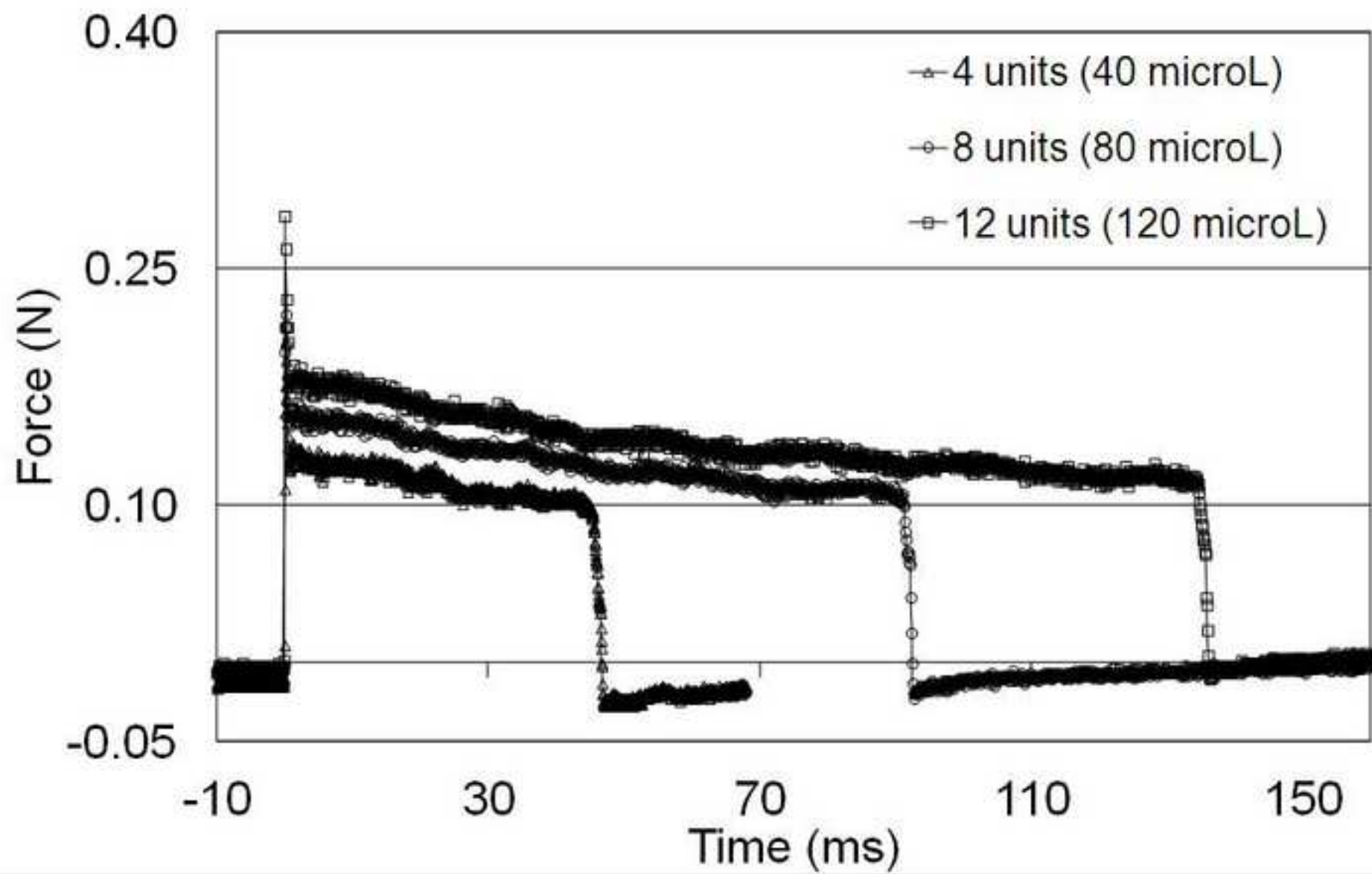
Figure(s)



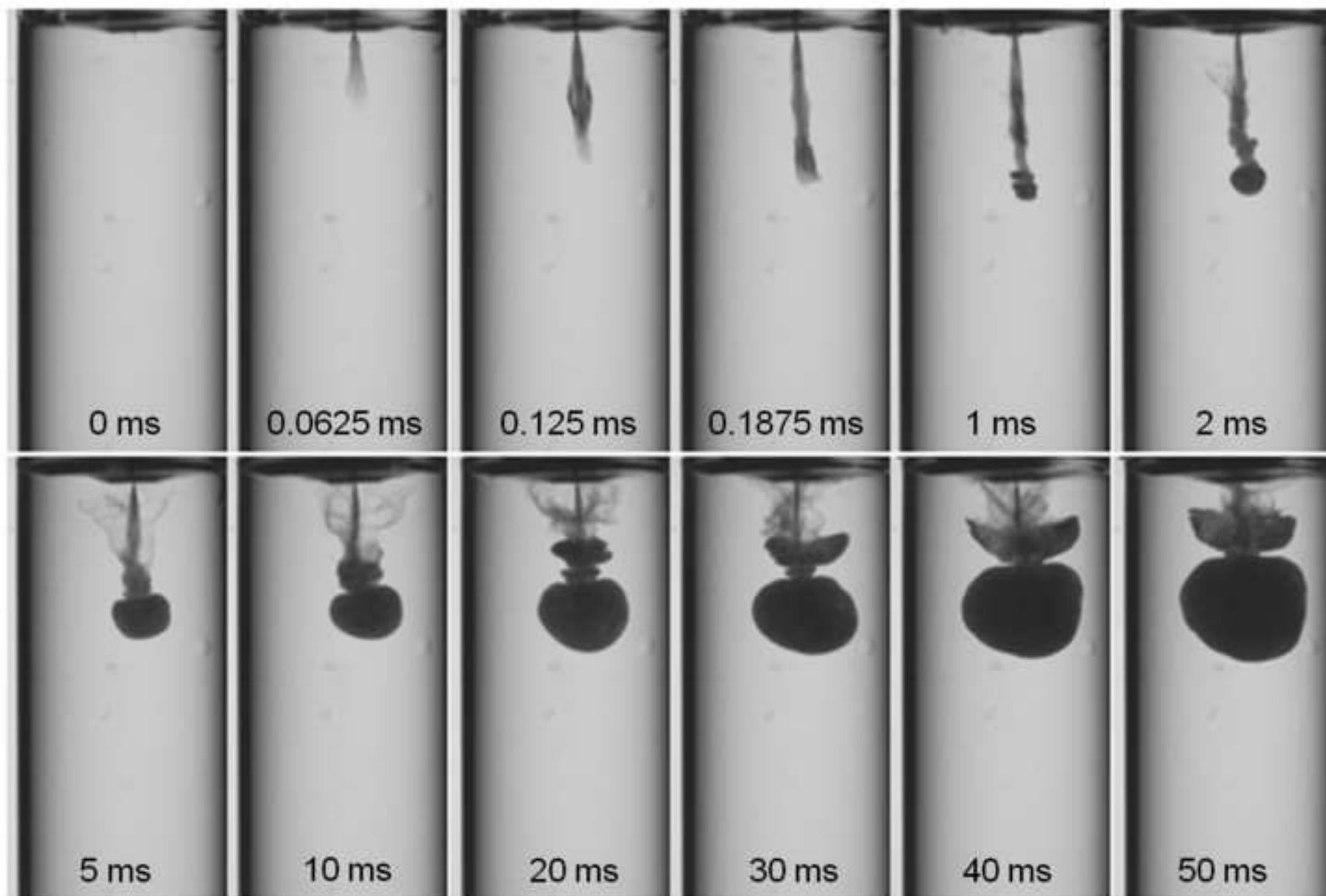
Figure(s)



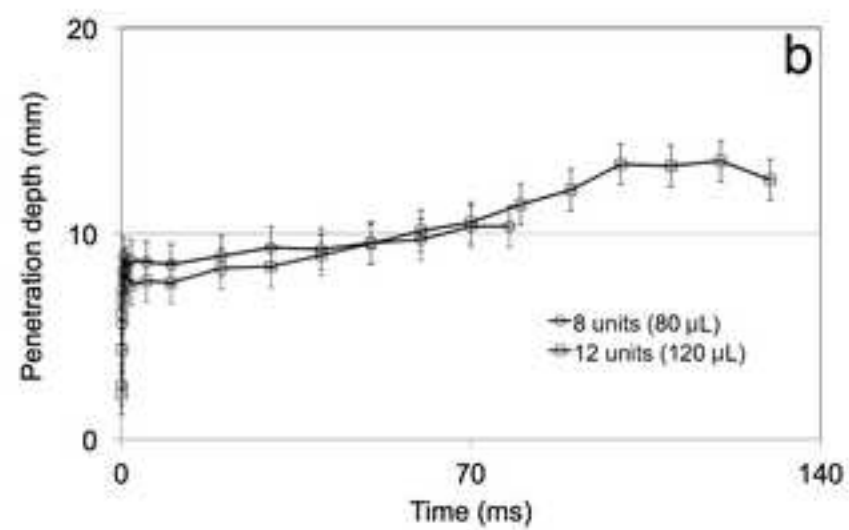
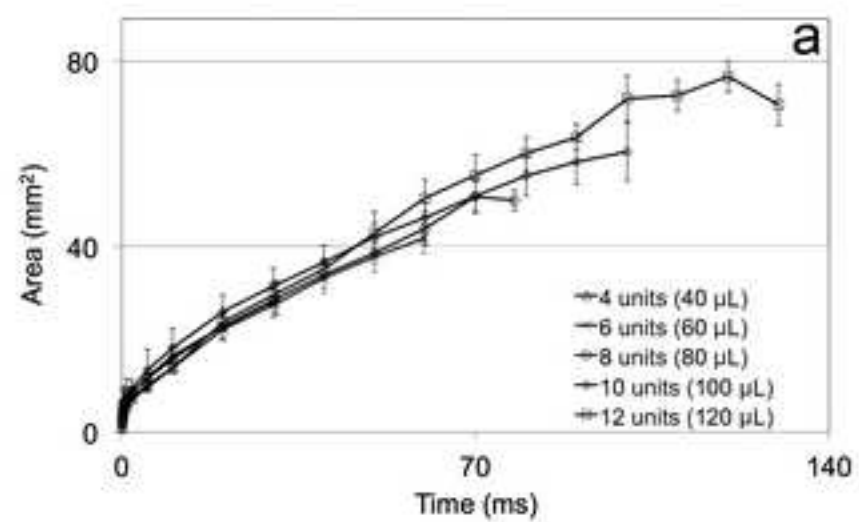
Figure(s)



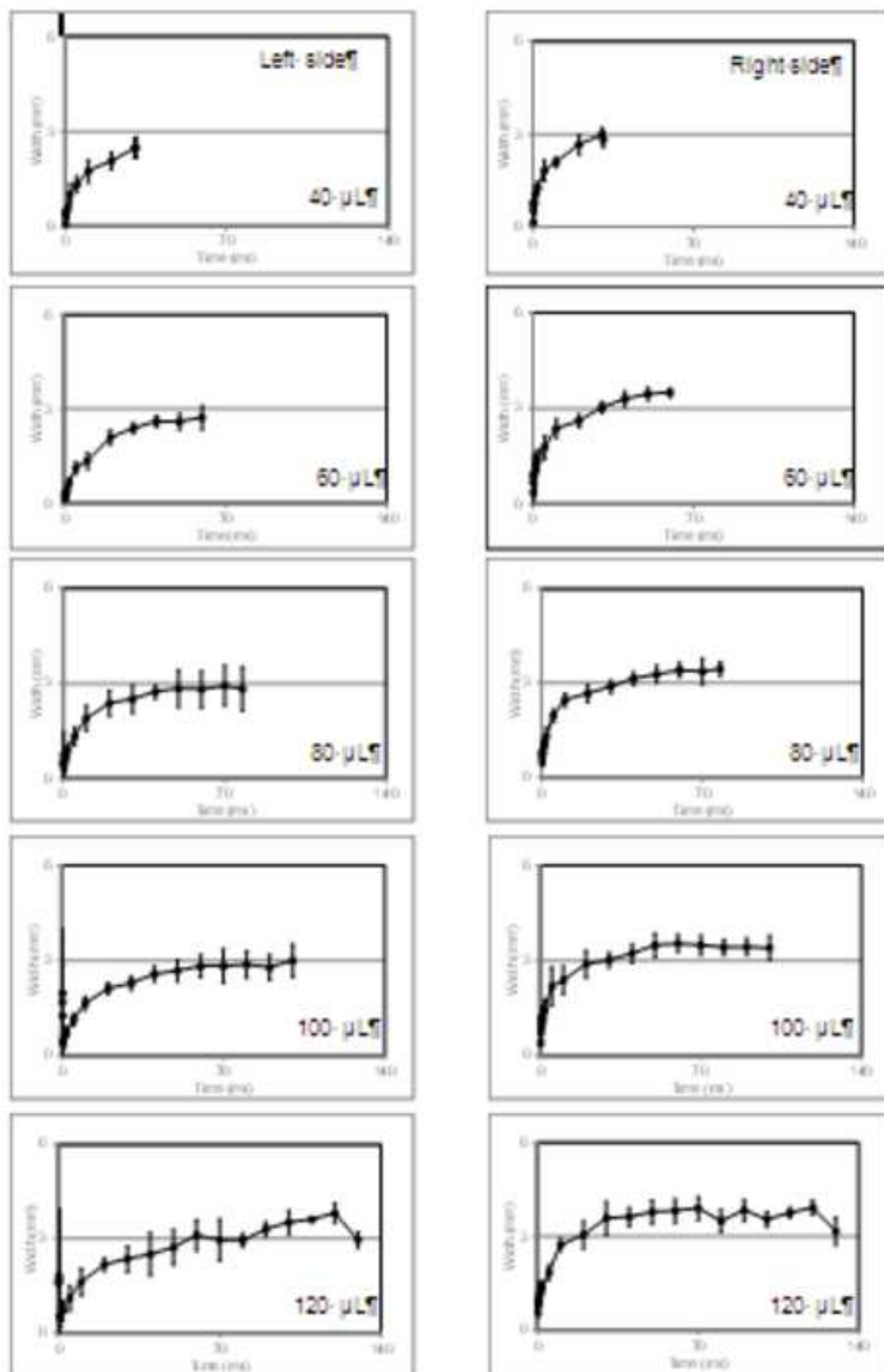
Figure(s)



Figure(s)



Figure(s)



Figure(s)

